Rapid Communications

Observation of nonscalar and logarithmic correlations in two- and three-dimensional percolation

Xiaojun Tan,[1,2] Romain Couvreur,[3,4,5,*] Youjin Deng,[1,2,†] and Jesper Lykke Jacobsen[3,4,5,‡]

[1]*Hefei National Laboratory for Physical Sciences at Microscale and Department of Modern Physics, University of Science and Technology of China, Hefei, Anhui 230026, China*

[2]*CAS Center for Excellence and Synergetic Innovation Center in Quantum Information and Quantum Physics, University of Science and Technology of China, Hefei, Anhui 230026, China*

[3]*Laboratoire de Physique de l'Ecole Normale Supérieure, ENS, Université PSL, CNRS, Sorbonne Université, Université Paris-Diderot, Sorbonne Paris Cité, Paris, France*

[4]*Sorbonne Université, École Normale Supérieure, CNRS, Laboratoire de Physique (LPENS), 75005 Paris, France*

[5]*Institut de Physique Théorique, Université Paris Saclay, CEA, CNRS, F-91191 Gif-sur-Yvette, France*

(Received 20 September 2018; published 21 May 2019)

In bulk percolation, we exhibit operators that insert N clusters with any given symmetry under the symmetric group $\mathcal{S}_N$. At the critical threshold, this leads to predictions that certain combinations of two-point correlation functions depend logarithmically on distance, without the usual power law. The behavior under rotations of certain amplitudes of correlators is also determined exactly. All these results hold in any dimension, $2 \leqslant d \leqslant 6$. Moreover, in $d = 2$ the critical exponents and universal logarithmic prefactors are obtained exactly. We test these predictions against extensive simulations of critical bond percolation in $d = 2$ and 3, for all correlators up to $N = 4$ ($d = 2$) and $N = 3$ ($d = 3$), finding excellent agreement. In $d = 3$ we further obtain precise numerical estimates for critical exponents and logarithmic prefactors.

DOI: 10.1103/PhysRevE.99.050103

Following Onsager's solution of the square-lattice Ising model [1], exact knowledge about two-dimensional (2D) statistical models is ever-growing. The algebraic use of symmetries—lattice duality [2], Yang-Baxter integrability [3,4], and local conformal invariance [5,6]—have propelled this impressive drive. The models solved encompass all of theoretical physics—from polymers [7], via cold atoms [8] and electron gases [9], to out-of-equilibrium transport in 1+1D [10,11]—and are matched by handsome experimental realizations [12–16].

The three-dimensional (3D) case has largely resisted similar efforts, due to the finiteness of the conformal group. The Zamolodchikov model [17,18] provides one of the scarce exceptions. Thanks to another algebraic structure [17,18] its partition function can be computed [19,20]. Unfortunately, it seems less experimentally relevant than its 2D cousins, and its more physical properties (correlation functions, critical exponents) remain elusive. Evidence of conformal symmetry was found in various models like the 3D Ising model [21] or percolation [22].

More recently, the study of conformal field theories (CFTs) in $d > 2$ has been thrusted into the limelight by the conformal bootstrap program. Using constraints of unitarity, this approach has led to new insights and improved the precision of critical exponents for local operators in the 3D Ising model [23]. Nonunitary extensions have given access to a few scaling dimensions in 3D (e.g., in the Yang-Lee model [24] or percolation [25]), but sometimes on the condition that an exponent was determined independently, either perturbatively [25] or numerically.

This Rapid Communication presents some exact results for bond percolation in both 2D and 3D, obtained by a different method. Percolation is a venerable physical model [26] with a host of practical applications [27], causing sustained interest [28]. At the critical threshold, it enjoys scale and conformal invariance, so one expects correlation functions to decay as power laws. However, the model is also nonunitary, due to its nonlocal observables, defined in terms of cluster connectivities [29]. Within the framework of logarithmic conformal field theory (LCFT), these nonlocal lattice observables are described by limits of local fields that may not be merely rescaled by dilatations, but linked among themselves in Jordan cell-like structures. Therefore, their correlators may also harbor *logarithmic* factors [30–32] reflecting the nondiagonalizability of the dilatation operator. The LCFT approach to $d > 2$ is complementary to the bootstrap in many respects: it focuses on nonlocal observables rather than local ones, and targets exact structural properties rather than bounds on the numerical values of exponents. To complete its predictions, one needs in particular to determine the scaling dimensions of the nonlocal observables by an independent means.

The nonlocal observables and the logarithmic correlators can be understood by treating percolation as the $Q \to 1$ limit of the Q-state Potts model [33,34]. Our approach hinges on a careful analysis [34,35] of its additional discrete $\mathcal{S}_Q$ permutation symmetry, present in any dimension d. References [35,36] classified the $\mathcal{S}_Q$ irreducible operators, related them to cluster observables, and unravelled the corresponding logarithmic contents. The set of predictions was greatly enhanced

*romain.couvreur@ens.fr
†yjdeng@ustc.edu.cn
‡jesper.jacobsen@ens.fr

in [37] by extending the initial treatment [35,36] of scalar operators (i.e., that transform trivially under rotations) to include also nonscalar operators that realize general representations of S_Q. We stress that these works and this Rapid Communication apply to *bulk* theories, which is more challenging [38–40] than its boundary counterpart [41,42].

In this Rapid Communication, we define nonlocal observables based on two-point functions of these operators. Their logarithmic structure is observed both in 2D and 3D, showing that exact predictions [37] hold for any d. The critical exponents and universal logarithmic prefactors (indecomposability parameters) are determined exactly in 2D and numerically in 3D. Moreover, the periodicity under rotations of correlator amplitudes is obtained exactly in 2D and 3D, and confirmed numerically. Our exact results add to the growing knowledge of higher-d percolation [28].

a. Percolation and the $Q \to 1$ Potts model. The partition function Z of the Q-state Potts model with interactions $-K\delta_{\sigma_i,\sigma_j}$ along edges, $(ij) \in E$, can be rewritten as the random cluster model [29,33]

$$Z = \sum_{A \subseteq E} Q^{k(A)} v^{|A|}. \tag{1}$$

Here $v = e^K - 1$, $|A|$ is the number of edges in the subset A, and $k(A)$ is the number of connected components (clusters) in the graph obtained by deleting lattice edges not in A. Note that (1) makes sense for $Q \in \mathbb{R}$ and gives access to nonlocal correlators of cluster connectivities. The limit $Q \to 1$ describes bond percolation.

The original interactions suppose $Q \in \mathbb{N}$ and have an $\mathcal{S}_Q$ symmetry. The classification of $\mathcal{S}_Q$ irreducible observables can nonetheless be analytically continued to $Q \in \mathbb{R}$, and leads to exact results on cluster correlators [35–37]. Below we study the probabilities that N clusters propagate from one neighborhood to another at the percolation threshold. We mainly use the bond percolation on the square and the simple-cubic (SC) lattice at their percolation thresholds $p_c(\text{square}) = 1/2$ [43] and $p_c(\text{SC}) = 0.248\,811\,85(10)$ [44–46]. To further check the universality of the critical exponents and particularly of the logarithmic prefactors, we also consider the triangular and the body-centered-cubic (BCC) lattice, with $p_c(\text{triangular}) = 2\sin(\pi/18)$ [47] and $p_c(\text{BCC}) = 0.180\,287\,62(20)$ [44,46].

b. Observables. Let $\mathcal{V}_i \equiv (i_1, i_2, \ldots, i_N)$ denote N mutually disconnected lattice sites in a small neighborhood. We usually take their positions to be aligned, $\mathbf{r}_{i_{m+1}} = \mathbf{r}_{i_m} + \boldsymbol{\delta}$, with $m = 1, 2, \ldots, N-1$. For $|\boldsymbol{\delta}| = 1$ they are nearest neighbors on square and cubic lattices. Let another site set $\mathcal{V}_j \equiv (j_1, j_2, \ldots, j_N)$ be distant from $\mathcal{V}_i$ by $\mathbf{r} = \mathbf{r}_j - \mathbf{r}_i$, with $r = |\mathbf{r}| \gg 1$. We consider configurations in which N distinct percolation clusters propagate from $\mathcal{V}_i$ to $\mathcal{V}_j$, i.e., each cluster connects a site in $\mathcal{V}_i$ to another site in $\mathcal{V}_j$. There are $N!$ such configurations, symbolically represented as (⁞⁞) and (X) for $N = 2$, (⁞⁞⁞), (⁞X), (X⁞), (XX), (XX), and (X) for $N = 3$, etc.

Appropriate linear combinations of the corresponding probabilities ($\mathbb{P}_{(⁞⁞)}$, $\mathbb{P}_{(X)}$, etc.) give access to the operator content of the underlying field theory [35,37]. More precisely, these combinations correspond, in the continuum limit, to the two-point function of an operator. This correspondence relies on the local $\mathcal{S}_N$ symmetry between the N spins of $\mathcal{V}_i$ (or $\mathcal{V}_j$), and the $\mathcal{S}_Q$ of the Potts model. Note that $\mathcal{S}_Q$ is subtly nontrivial, since percolation is not $Q = 1$ but rather $Q \to 1$. The definitions of observables acting on $N = 2$ and $N = 3$ spins are recalled below. Each of them corresponds, technically, to a pair of Young diagrams for $\mathcal{S}_N$ and $\mathcal{S}_Q$ [37].

Consider first observables describing the propagation of $N = 2$ clusters. There are two different combinations, corresponding to the symmetric and antisymmetric Young diagrams of $\mathcal{S}_2$,

$$\mathbb{P}_{2\text{s}} = \mathbb{P}_{(⁞⁞)} + \mathbb{P}_{(X)} \qquad \mathbb{P}_{2\text{a}} = \mathbb{P}_{(⁞⁞)} - \mathbb{P}_{(X)}\,,$$

corresponding in the continuum limit to the two-point functions of two operators $\mathcal{O}_{2\text{s}}$ and $\mathcal{O}_{2\text{a}}$. Below, we also use the term observable to describe a two-point function. The scaling dimensions of these operators in 2D CFTs are known [37] and $\mathcal{O}_{2\text{s}}$ ($\mathcal{O}_{2\text{a}}$) transforms trivially (nontrivially) under rotations.

For $N = 3$ clusters, the relevant combinations are

$$\begin{aligned}
\mathbb{P}_{3\text{s}} &= \mathbb{P}_{(⁞⁞⁞)} + \mathbb{P}_{(⁞X)} + \mathbb{P}_{(X⁞)} + \mathbb{P}_{(XX)} + \mathbb{P}_{(XX)} + \mathbb{P}_{(X)} \\
\mathbb{P}_{3\text{m}} &= 2\mathbb{P}_{(⁞⁞⁞)} + \mathbb{P}_{(⁞X)} + \mathbb{P}_{(X⁞)} - \mathbb{P}_{(XX)} - \mathbb{P}_{(XX)} - 2\mathbb{P}_{(X)} \\
\mathbb{P}_{3\text{a}} &= \mathbb{P}_{(⁞⁞⁞)} - \mathbb{P}_{(⁞X)} - \mathbb{P}_{(X⁞)} + \mathbb{P}_{(XX)} + \mathbb{P}_{(XX)} - \mathbb{P}_{(X)}\,,
\end{aligned}$$

where $\mathbb{P}_{N\circ}$ (with subscript $\circ = \text{s}, \text{m}, \text{a}$) refers to the symmetric, mixed, and antisymmetric Young diagram of $\mathcal{S}_3$. For $N = 4$, we have $\mathbb{P}_{4\text{s}}$, $\mathbb{P}_{4\text{m1}}$, $\mathbb{P}_{4\text{m2}}$, $\mathbb{P}_{4\text{m3}}$, and $\mathbb{P}_{4\text{a}}$, since $\mathcal{S}_4$ admits five Young diagrams [see the Supplemental Material (SM) for details [48]]. All these observables are two-point functions, and their definitions are independent of the Q value. They are expected to decay algebraically at criticality, as $r^{-2\Delta}$, with (*a priori*) distinct, symmetry-dependent scaling dimensions.

c. Critical exponents in 2D. In 2D, the exponents can be computed exactly using algebraic methods and CFT results. They are expressed in terms of conformal weights $h_{r,s}$ in the so-called Kac parametrization

$$h_{r,s} = \frac{[r(x+1) - sx]^2 - 1}{4x(x+1)}, \tag{2}$$

where x determines Q by $\sqrt{Q} = 2\cos\frac{\pi}{x+1}$ (so $x = 2$ for percolation), and (r, s) are Kac labels.

The exponents of the above observables were already studied in [37], but in the geometry of an infinite cylinder, suitable for transfer matrix (TM) computations. In that case, $\mathcal{V}_i$ ($\mathcal{V}_j$) reside at the lower (upper) rim of the cylinder. Since moreover clusters cannot cross, certain configurations cannot be realized on the cylinder. In this Rapid Communication we perform Monte Carlo (MC) computations in a physically more relevant geometry of the plane. This alleviates these restrictions, leading in some cases to changes in the exponents.

On the cylinder, the symmetry $\mathcal{S}_N$ is effectively restricted to its subgroup of cyclic permutations $\mathcal{C}_N$. The scaling dimension related to the one-dimensional representation $\exp(i2\pi p/N)$ of $\mathcal{C}_N$ was found to be [37]

$$\Delta_{p,N} = h_{p/N,N} + h_{-p/N,N}, \tag{3}$$

where p is an integer between $\lfloor -N/2 \rfloor$ and $\lfloor N/2 \rfloor$ determined as follows: For the Young diagram of a given operator, find all

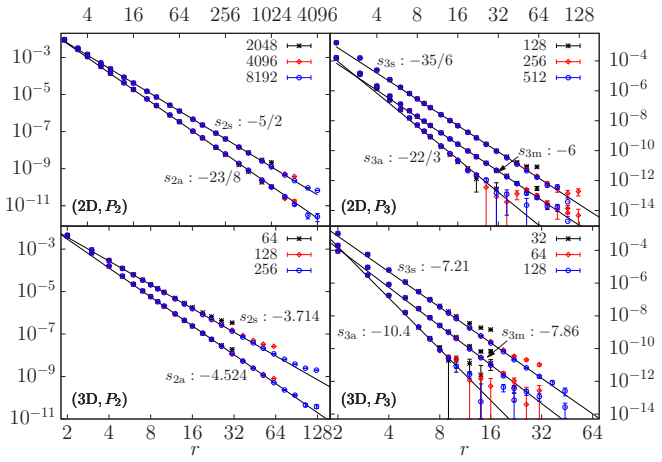

FIG. 1. Log-log plot of $\mathbb{P}_{2\circ}$ and $\mathbb{P}_{3\circ}$ versus distance r in 2D (square) and 3D (SC), for different system sizes L. Subscripts $\circ = \mathrm{s}, \mathrm{m}, \mathrm{a}$ refer to symmetric, mixed, and antisymmetric correlators. Straight lines with slope s come from the least-squares fits. For clarity, $\mathbb{P}_{3\mathrm{s}}$ ($\mathbb{P}_{3\mathrm{m}}$) have been multiplied by a factor 5 (2).

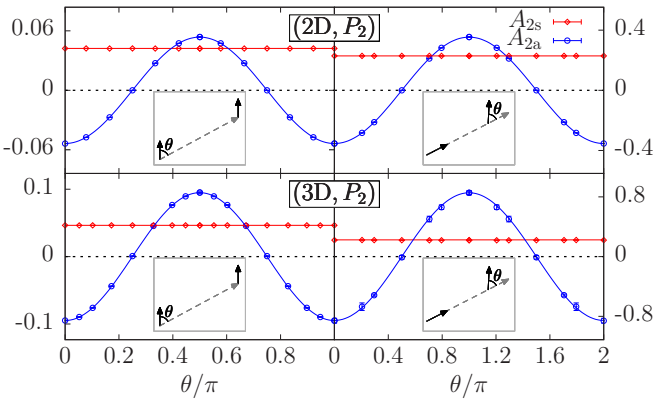

FIG. 2. Rotational dependence of $\mathbb{P}_{2s} r^{2\Delta_{2s}}$ and $\mathbb{P}_{2a} r^{2\Delta_{2a}}$. The results are obtained from extrapolation first to $L \to \infty$ and then to $r \to \infty$. For both ways of rotations shown in the insets, the symmetric correlation $\mathbb{P}_{2s}$ is independent of rotation angle θ, while the asymmetric one $\mathbb{P}_{2a}$ is proportional to $\cos(2\theta + \pi)$ or $\cos(\theta + \pi)$.

its corresponding standard Young tableaux and compute for each of them its index $\mathcal{I}$ (= sum of descents). The p in (3) is then the value of $\mathcal{I} \bmod N$ leading to the smallest $\Delta_{p,N}$ (most relevant contribution).

Consider first the $N = 2$ observables. The scaling dimensions of $\mathcal{O}_{2\mathrm{s}}$ and $\mathcal{O}_{2\mathrm{a}}$ are $\Delta_{2\mathrm{s}} = 2h_{0,2} = 5/4$ and $\Delta_{2\mathrm{a}} = h_{1/2,2} + h_{-1/2,2} = 23/16$. The leading behavior of the probabilities are then $\mathbb{P}_{2\mathrm{s}} \propto r^{-2\Delta_{2\mathrm{s}}}$ and $\mathbb{P}_{2\mathrm{a}} \propto r^{-2\Delta_{2\mathrm{a}}}$. These predictions were checked by TM on the cylinder [37], and they are confirmed by our MC computations in the plane (upper-left panel of Fig. 1 and Table I). More precisely, the least-squares fits give $(\Delta_{2\mathrm{s}}, \Delta_{2\mathrm{a}}) = (1.2503 \pm 0.0006, 1.438 \pm 0.004)$ for the square lattice and $(1.2504 \pm 0.0006, 1.445 \pm 0.010)$ for the triangular lattice.

The $N = 3$ case is more interesting, since the restriction from $\mathcal{S}_3$ to $\mathcal{C}_3$ does not necessarily hold in the geometry relevant for MC. In particular, both (⫼) and (✕) can generically be realized in the plane, while on the cylinder one of them cannot. To be in the generic situation, the points in $\mathcal{V}_i$ and $\mathcal{V}_j$ must be sufficiently spaced, and we henceforth assume this is the case. In this case, the restriction from $\mathcal{S}_N$ to $\mathcal{C}_N$—a key argument in deriving (3)—does not occur. But remarkably, (3) still appears to provide the correct scaling dimension, provided p is chosen differently (see below).

TABLE I. Least-squares fitting results for N-cluster exponents Δ in 2D and 3D. The rows "Theo." are for the exact values from the $d = 2$ LCFT, as calculated from (2) and (3) with index (p, N).

2D	$\Delta_{2\mathrm{s}}$	$\Delta_{2\mathrm{a}}$	$\Delta_{3\mathrm{s}}$	$\Delta_{3\mathrm{m}}$	$\Delta_{3\mathrm{a}}$
	1.2503(6)	1.438(4)	2.93(4)	2.986(14)	3.75(20)
Theo.	5/4	23/16	35/12	3	11/3
(p, N)	(0,2)	(1,2)	(0,3)	(1,3)	(3,3)
2D	$\Delta_{4\mathrm{s}}$	$\Delta_{4\mathrm{m1}}$	$\Delta_{4\mathrm{m2}}$	$\Delta_{4\mathrm{m3}}$	$\Delta_{4\mathrm{a}}$
	5.24(3)	5.25(10)	5.40(10)	5.60(20)	7.00(30)
Theo.	21/4	339/64	87/16	363/64	111/16
(p, N)	(0,4)	(1,4)	(2,4)	(3,4)	(6,4)
3D	$\Delta_{2\mathrm{s}}$	$\Delta_{2\mathrm{a}}$	$\Delta_{3\mathrm{s}}$	$\Delta_{3\mathrm{m}}$	$\Delta_{3\mathrm{a}}$
	1.857(2)	2.262(10)	3.605(8)	3.93(4)	5.2(2)

The case of the symmetric operator $\mathcal{O}_{3\mathrm{s}}$ presents no such subtleties. Its corresponding Young diagram has one index $\mathcal{I} = 0$, and setting $p = 0$ in (3) we find $\Delta_{3\mathrm{s}} = 2h_{0,3} = 35/12$. This coincides with the well-known six-leg watermelon operator [49] and agrees well with the MC results for $\mathbb{P}_{3\mathrm{s}}$ [upper-right panel of Fig. (1) and and Table I]. Similarly, for $\mathcal{O}_{3\mathrm{m}}$ we find $p = 1$, and $\Delta_{3\mathrm{m}} = h_{1/3,3} + h_{-1/3,3} = 3$ agrees with the numerics for $\mathbb{P}_{3\mathrm{m}}$. The interesting case concerns $\mathcal{O}_{3\mathrm{a}}$, for which $\mathcal{I} = 3$. On the cylinder, one finds the *same* scaling dimension as for $\mathcal{O}_{3\mathrm{s}}$, namely, $\Delta_{0,3} = 35/12$, since $p = \mathcal{I} \bmod N = 0$. However, our MC results in the plane unambiguously agree with $\Delta_{3,3} = 11/3$. We hypothesize that exact results in the plane are obtained by setting $p = \mathcal{I}$ (without mod N). This is confirmed by an exhaustive study of the five $N = 4$ exponents (see SM [48] and Table I).

d. Critical exponents in 3D. The definitions of the observables are independent of d. The corresponding operators are only quasiprimary in 3D, but the various probabilities $\mathbb{P}$ should still scale with distinct scaling dimensions, due to their different symmetry content. This is confirmed by our MC results (bottom panels of Fig. 1 and Table I). Nonlocal observables of this type do not appear to have been previously studied in 3D.

e. Conformal spin. Observables that are not fully symmetric transform nontrivially under local rotations. We first illustrate this in 2D, where the conformal spin of operators corresponding to (3) is $|h_{p/N,N} - h_{-p/N,N}| = p$. Thus, the $N = 2$ operators $\mathcal{O}_{2s}$ and $\mathcal{O}_{2a}$ have spin 0 and 1, respectively.

This can be checked in MC simulations, using techniques similar to [37]. We perform a rotation of $\mathcal{V}_i$ around $\mathcal{V}_j$, while keeping the local orientation of each site in the neighborhoods fixed. The upper-left panel of Fig. 2 shows the renormalized amplitude of the observables as a function of the angle. It is clear that in the large-r limit the two-point function of $\mathcal{O}_{2s}$ is invariant under rotations, whereas the two-point function of $\mathcal{O}_{2a}$ fits perfectly with $\propto \cos(2\theta + \pi)$. Another way to

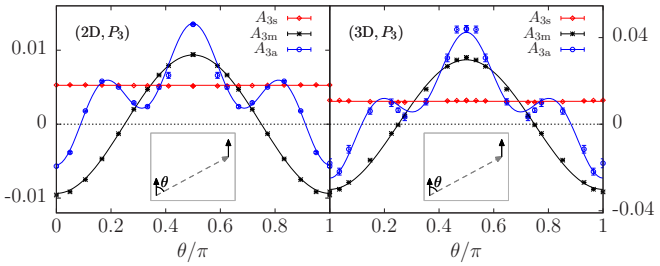

FIG. 3. Rotational dependence of $\mathbb{P}_{3s} r^{2\Delta_{3s}}$, $\mathbb{P}_{3m} r^{2\Delta_{3m}}$, and $\mathbb{P}_{3a} r^{2\Delta_{3a}}$. The rotation schemes are given in the insets. The simulation parameters are $(L, r) = (8192, 12)$ in 2D and (512,9) in 3D. To have a better view, the $\mathbb{P}_{3m}$ data are rescaled by a factor of 0.22 in 3D.

investigate the spin is to keep $\mathcal{V}_i$ around $\mathcal{V}_j$ fixed, but do a local rotation of the relative position $\boldsymbol{\delta}$ in one of them. In CFT, this corresponds to a simple conformal change of the metric around one point. The results match now $\propto \cos(\theta + \pi)$ for the spin-1 case (top-right panel Fig. 2). The factor 2 difference of the periods is understood (see [37] for details).

In 3D, we cannot compute the conformal spin from (3), but on general grounds we expect it to be independent of d. This is confirmed by the bottom panels of Fig. 2 that show the same two protocols as above, but now in 3D.

The $N = 3$ observables can be investigated in the same way. In 2D, the prediction is that $\mathcal{O}_{3s}$ has spin 0, while $\mathcal{O}_{3m}$ has spin 1, and $\mathcal{O}_{3a}$ has spin 3 in the plane and spin 0 on the cylinder. For numerical and practical reasons, we only investigated the first of the above protocols (the second being much more challenging for $N = 3$, given the constraints of the square lattice). The results are shown in Fig. 3. The spins of $\mathcal{O}_{3s}$ and $\mathcal{O}_{3m}$ are seen to be 0 and 1, respectively [we find $\mathbb{P}_{3m} \propto \cos(2\theta + \pi)$], in agreement with the 2D CFT predictions. The prediction for $\mathcal{O}_{3a}$ is spin 3, but instead of a "pure" function of the form $\cos(2s\theta)$ with $s = 3$, $\mathbb{P}_{3a}$ is seen to be a mixed sum

$$\mathbb{P}_{3a} \propto \cos(2\theta) + A_1 \cos(4\theta) + A_2 \cos(6\theta),$$

where A_1 and A_2 are nonuniversal amplitudes. In general, we expect the angular dependence of the two-point function of a spin-s operator to be a sum of the form $\sum_{k=1}^{s} b_k \cos(2k\theta)$, where the b_k are nonuniversal. For all three observables, we obtain the same spin in 3D as in 2D, as expected.

f. Logarithmic features. An important breakthrough of [35] was to prove the possibility of studying LCFTs through a limiting procedure. In this class of theories—which includes percolation—there exist operators whose two-point functions are not purely a power law. In 2D, they have a logarithmic dependence of the form

$$\langle \mathcal{O}_\Delta(0)\mathcal{O}_\Delta(r)\rangle = -\frac{2b \ln r}{r^{2\Delta}}, \tag{4}$$

where Δ is the scaling dimension and b is called an indecomposability parameter. The operator $\mathcal{O}_\Delta$ has a logarithmic partner, hence it cannot be normalized independently. The indecomposability parameter is believed to be universal and exact results are known for its value in many cases [31,38,39,41].

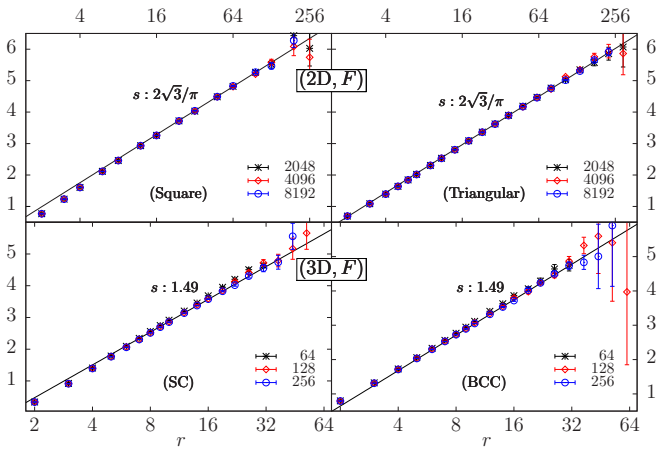

FIG. 4. Semilogarithmic plot of the logarithmic correlation $F(r)$ for different 2D and 3D lattices. The slopes of the straight lines are universal (independent of lattice type), and their values are respectively $\delta(2D) = 2\sqrt{3}/\pi$ and $\delta(3D) = 1.49(3)$.

For a LCFT to result as a limit of ordinary CFTs, the scaling dimensions of two operators must collide in the limit. This is exactly what happens for percolation in *any* dimensions: the scaling dimensions of the local energy operator ε and of the symmetric two-cluster operator $\mathcal{O}_{2s}$ collide when $Q \to 1$. This is accompanied by a divergence in the two-point function of $\mathcal{O}_{2s}$, which can be removed by mixing the two operators into a Jordan cell. The parameter b is proportional to the quantity

$$\delta = 2 \times \lim_{Q\to 1} \frac{\Delta_2 - \Delta_\varepsilon}{Q - 1}. \tag{5}$$

This universal number characterizes both the LCFT at $Q = 1$ and the limit of CFTs when $Q \to 1$.

It is possible to go further and isolate the logarithmic factor in (4). For $N = 2$, let $\mathbb{P}_0 \equiv \mathbb{P}_{(\bullet\bullet)}$ be the probability each of the four specified points belongs to a different percolation cluster; let $\mathbb{P}_1$ be the probability that the points belong to three different clusters, one of which propagates from one site in $\mathcal{V}_i$ to another site in $\mathcal{V}_j$, viz., $\mathbb{P}_1 \equiv \mathbb{P}_{(\bullet\bullet)} + \mathbb{P}_{(\bullet\bullet)} + \mathbb{P}_{(\bullet\bullet)} + \mathbb{P}_{(\bullet\bullet)}$. Note that $\mathbb{P}_{(\bullet\bullet)}$ increases with r and converges to $(\mathbb{P}_{\neq})^2$ for $r \to \infty$, where $\mathbb{P}_{\neq}$ is the probability that the two points in $\mathcal{V}_i$ belong to different percolation clusters. The main result of [35] is that the composite observable

$$F(r) = \frac{\mathbb{P}_0(r) + \mathbb{P}_1(r) - (\mathbb{P}_{\neq})^2}{\mathbb{P}_{2s}(r)} \sim \delta \ln(r) \tag{6}$$

diverges as a pure logarithm. Crucially, the predictions (5) and (6), as well as $\Delta_2 = \Delta_\varepsilon$ exactly at $Q = 1$, hold in both 2D and 3D. In 2D we know also $\Delta_2(Q) = 2h_{2,1}$ and $\Delta_\varepsilon(Q) = 2h_{0,2}$ so $\delta = 2\sqrt{3}/\pi \approx 1.10266\ldots$.

In the numerics we take each of $\mathcal{V}_i$ and $\mathcal{V}_j$ to contain a pair of nearest-neighbor sites for the square, SC, and BCC lattices and of next-nearest-neighbor sites for the triangular lattice. From the least-squares fit of the data in Fig. 4, we obtain $\delta(\text{square}) = 1.12(3)$ and $\delta(\text{triangular}) = 1.11(2)$, improving the numerics in [35], and very close to the exact result. The

3D logarithmic scaling in (6) is confirmed very clearly in the right panel of Fig. 4, and we find $\delta(\mathrm{SC}) = 1.53(3)$ and $\delta(\mathrm{BCC}) = 1.49(3)$. Of course, $\Delta_2(Q)$ and $\Delta_\varepsilon(Q)$ are not known analytically in 3D. We can nonetheless give a rough estimate of δ from (5) by using the numerical values $\Delta_2 \approx 2.243(2)$ and $\Delta_\varepsilon \approx 1.413(1)$ for the 3D Ising model ($Q = 2$) [50,51]. This gives $\delta \approx 2[\Delta_2(Q=2) - \Delta_\varepsilon(Q=2)] = 1.66$. The agreement with the estimated values of $\delta(3\mathrm{D})$ is surprisingly good, showing that $\Delta_2(Q)$ and $\Delta_\varepsilon(Q)$ have little curvature (as in 2D).

Figure 4 clearly demonstrates the universality of the logarithmic prefactors in both 2D and 3D.

g. Numerical details. Our simulations use toroidal boundary conditions, and linear system sizes vary from $L = 8$ to 8192 in 2D and 512 in 3D. It is especially challenging that the correlators decay very rapidly with r, in particular for $N = 3$ and 4. For instance, $\mathbb{P}_{3a}$ decays with exponent $2\Delta_{3a}(3\mathrm{D}) \approx 10.4$, so $\mathbb{P}_{3a} \leqslant 10^{-14}$ already for $r \approx 24$ (see Fig. 1). Thus, reliable data are only available for a small range of r and L, calling for careful finite-size analysis. Since most CPU time is spent measuring, independent simulations are performed for each N. In total, we used $\approx 2 \times 10^6$ CPU core hours.

Data for $N = 2, 3$ (on square and SC lattices) are partly shown in Fig. 1, and fitted to $\mathcal{O}(r)|_L = r^{-2\Delta_\mathcal{O}}(a + b_1 r^{-1} + b_2 r^{-2})$ by the least-squares criterion. For fixed L, we impose cutoffs, $r_{\min} \leqslant r \leqslant r_{\max}$, on the data admitted in the fit, and we study the effect on the residual χ^2 of varying $r_{\min}$ and $r_{\max}$. Results are then extrapolated to $L \to \infty$. To avoid simultaneous finite-r and finite-L corrections, we also simulate $r = \alpha L$, with $0 < \alpha < 1$ constant. Those data are fitted by $\mathcal{O}(L) = (\alpha L)^{-2\Delta_\mathcal{O}}(a + b_1 L^{-1} + b_2 L^{-2})$. Final results are reported in Table I, where the quoted error bars include systematic uncertainties.

h. Discussion and outlook. To summarize, we gave exact predictions about the geometry of percolation clusters in 2D and 3D, with numerical checks. In 3D we gave estimates for new exponents, and theoretical predictions [35] of the logarithmic structure were verified. We found that the rotational behavior of correlators is similar in 3D and 2D, with spin $s = p$ in both cases. While our analysis was confined to percolation, it proves the avail of studying LCFT as a limit of ordinary CFT. Being one of the few methods to study LCFT in higher dimensions, we believe it opens the possibility to derive exact results in 3D for a wider range of models, such as the cluster formulation of the Ising model or self-avoiding walks.

Acknowledgments. X.T. and Y.D. acknowledge the support by National Natural Science Foundation of China (Grant No. 11625522) and the Ministry of Science and Technology of China (Grant No. 2016YFA0301604). R.C. and J.L.J. were supported by the ERC Advanced Grant NuQFT.

[1] L. Onsager, Phys. Rev. **65**, 117 (1944).
[2] H. A. Kramers and G. H. Wannier, Phys. Rev. **60**, 252 (1941).
[3] E. H. Lieb, Phys. Rev. Lett. **18**, 692 (1967).
[4] R. J. Baxter, Ann. Phys. (NY) **70**, 193 (1972).
[5] A. A. Belavin, A. M. Polyakov, and A. B. Zamolodchikov, Nucl. Phys. B **241**, 333 (1984).
[6] D. Friedan, Z. Qiu, and S. Shenker, Phys. Rev. Lett. **52**, 1575 (1984).
[7] B. Duplantier and H. Saleur, Nucl. Phys. B **290**, 291 (1987).
[8] E. H. Lieb and W. Liniger, Phys. Rev. **130**, 1605 (1963).
[9] R. Couvreur, E. Vernier, J. L. Jacobsen, and H. Saleur, Nucl. Phys. **941**, 507 (2019).
[10] B. Derrida, M. R. Evans, V. Hakim, and V. Pasquier, J. Phys. A: Math. Gen. **26**, 1493 (1993).
[11] A. Lazarescu, J. Phys. A: Math. Theor. **46**, 145003 (2013).
[12] K. v. Klitzing, G. Dorda, and M. Pepper, Phys. Rev. Lett. **45**, 494 (1980).
[13] H. Moritz, T. Stöferle, M. Köhl, and T. Esslinger, Phys. Rev. Lett. **91**, 250402 (2003).
[14] B. Paredes, A. Widera, V. Murg, O. Mandel, S. Fölling, I. Cirac, G. V. Shlyapnikov, T. W. Hänsch, and I. Bloch, Nature (London) **429**, 277 (2004).
[15] X.-W. Guan, M. T. Batchelor, and C. Lee, Rev. Mod. Phys. **85**, 1633 (2013).
[16] B. Maier and J. O. Rädler, Phys. Rev. Lett. **82**, 1911 (1999).
[17] A. B. Zamolodchikov, Zh. Eksp. Teor. Fiz. **79**, 641 (1980).
[18] A. B. Zamolodchikov, Commun. Math. Phys. **79**, 489 (1981).
[19] R. J. Baxter, Commun. Math. Phys. **88**, 185 (1983).
[20] R. J. Baxter, Physica D **18**, 321 (1986).
[21] C. Cosme, J. M. V. P. Lopes, and J. Penedones, J. High Energy Phys. 08 (2015) 022.
[22] G. Gori and A. Trombettoni, J. Stat. Mech.: Theory Exp. (2015) P07014.
[23] S. El-Showk, M. F. Paulos, D. Poland, S. Rychkov, D. Simmons-Duffin, and A. Vichi, Phys. Rev. D **86**, 025022 (2012).
[24] F. Gliozzi and A. Rago, J. High Energy Phys. 10 (2014) 042.
[25] A. LeClair and J. Squires, J. Stat. Mech. (2018) 123105.
[26] S. R. Broadbent and J. M. Hammersley, Math. Proc. Cambridge Philos. Soc. **53**, 629 (1957).
[27] D. Stauffer and A. Aharony, *Introduction to Percolation Theory,* revised 2nd ed. (Taylor and Francis, London, 1994).
[28] N. Araújo, P. Grassberger, B. Kahng, K. Schrenk, and R. Ziff, Eur. Phys. J. **223**, 2307 (2014).
[29] C. M. Fortuin and P. W. Kasteleyn, Physica **57**, 536 (1972).
[30] V. Gurarie, Nucl. Phys. B **410**, 535 (1993).
[31] V. Gurarie and A. W. W. Ludwig, J. Phys. A: Math. Gen. **35**, L377 (2002).
[32] A. M. Gainutdinov, J. L. Jacobsen, N. Read, H. Saleur, and R. Vasseur, J. Phys. A: Math. Theor. **46**, 494012 (2013).
[33] F. Y. Wu, Rev. Mod. Phys. **54**, 235 (1982).
[34] J. Cardy, arXiv:cond-mat/9911024.
[35] R. Vasseur, J. L. Jacobsen, and H. Saleur, J. Stat. Mech.: Theory Exp. (2012) L07001.
[36] R. Vasseur and J. L. Jacobsen, Nucl. Phys. B **880**, 435 (2014).
[37] R. Couvreur, J. L. Jacobsen, and R. Vasseur, J. Phys. A: Math. Theor. **50**, 474001 (2017).
[38] A. M. Gainutdinov, N. Read, H. Saleur, and R. Vasseur, J. High Energy Phys. 05 (2015) 114.

[39] R. Vasseur, A. M. Gainutdinov, J. L. Jacobsen, and H. Saleur, Phys. Rev. Lett. **108**, 161602 (2012).
[40] J. L. Jacobsen and H. Saleur, J. High Energ. Phys. 01 (2019) 084.
[41] R. Vasseur, J. L. Jacobsen, and H. Saleur, Nucl. Phys. B **851**, 314 (2011).
[42] G. Gori and J. Viti, Phys. Rev. Lett. **119**, 191601 (2017).
[43] H. Kesten, Commun. Math. Phys. **74**, 41 (1980).
[44] C. D. Lorenz and R. M. Ziff, Phys. Rev. E **57**, 230 (1998).
[45] J. Wang, Z. Zhou, W. Zhang, T. M. Garoni, and Y. Deng, Phys. Rev. E **87**, 052107 (2013).
[46] X. Xu, J. Wang, J.-P. Lv, and Y. Deng, Frontiers Phys. **9**, 113 (2014).
[47] M. F. Sykes and J. W. Essam, J. Math. Phys. **5**, 1117 (1964).
[48] See Supplemental Material at http://link.aps.org/supplemental/10.1103/PhysRevE.99.050103 for a discussion of the $N = 4$ observables and additional simulation details.
[49] H. Saleur and B. Duplantier, Phys. Rev. Lett. **58**, 2325 (1987).
[50] Y. Deng and H. W. J. Blöte, Phys. Rev. E **70**, 056132 (2004).
[51] A. M. Ferrenberg, J. Xu, and D. P. Landau, Phys. Rev. E **97**, 043301 (2018).